Nanofabrication (2022) 7, 11-23
https://doi.org/10.37819/nanofab.007.250

eurasia

ORIGINAL ARTICLE

Check for updates

Quantifying the differences in properties between polycrystals containing planar and curved grain boundaries

Robert M. Forrest[a]; Emanuel A. Lazar[b]; Saurav Goel[c,d+]; Jonathan J. Bean[a]*

[a]*Department of Materials Science and Metallurgy, The University of Cambridge, Cambridge, CB3 0FS, UK*
[b]*Department of Mathematics, Bar-Ilan University, Ramat Gan 5290002, Israel*
[c]*School of Engineering, London South Bank University, 103 Borough Road, London SE10AA, UK*
[d]*Department of Mechanical Engineering, University of Petroleum and Energy Studies, Dehradun, India.*
*Corresponding authors: [+]S. Goel (GOELS@Lsbu.ac.uk) and *J.J. Bean (jb2191@cam.ac.uk)*

ABSTRACT

There are several methods in which grain boundaries can be made for modelling, but most produce planar (flat) grains. In this study, we investigated the difference in materials properties between polycrystalline systems comprised of planar grain and curved grain boundaries. Several structural and mechanical properties for both systems were determined. For systems with curved grain boundaries, it was found that the elastic moduli are all larger in magnitude, the excess volumes are comparable, and the plastic properties are smaller. In addition, a grain tracking algorithm was used to determine the differences in the numbers of triple junctions detected between polycrystalline systems with planar and curved grain boundaries. This can be theoretically determined and compared to a simple model system. We find that planar systems of grain boundaries possess significantly more triple junctions than systems of curved grain boundaries by a factor of two. There are also systematic differences between the two types of a system when they undergo grain growth, when there is an anomalous close-packed hexagonal phase which grows in the system of planar grain boundaries.

ARTICLE HISTORY

Received: 28-08-2022
Revised: 11-11-2022
Accepted: 23-11-2022

KEYWORDS

MD simulation; polycrystalline; materials; characterisation

1. Introduction

Metals are one of the most important classes of materials in the modern world, with steel alone accounting for over 2,000 million metric tonnes of production in 2020, the crystal structure of metals is far from perfect, and they usually contain several different types of defects, including point defects, dislocations, grain boundaries and voids (Ashby & Jones, 2011). Materials containing defects such as those are called polycrystalline, and the nature in which the defects manifest themselves is called the microstructure (Jones & Ashby, 2012). Understanding the microstructure of materials is extremely important in creating safe materials for aircraft, automobiles, and other structural applications (Ashby, 1994) because crystal defects largely control the mechanical performance and failure modes of materials (Sutton & Materials, 1995). One of the most striking examples of this is when comparing a material's theoretical maximum yield stress to experimental reproductions, in which a difference of at least two orders of magnitude has been detected. The root cause for the discrepancy between theoretical and experimental properties has been largely attributed to dislocations.

However, the effect of other defects, such as grain boundaries, cannot be discounted (Hirth, 1985; Orowan, 1934).

Atomistic modelling seeks to determine the structure and properties of a material based on a knowledge of the atoms alone. It is a powerful technique because it can investigate the phenomena of interest. However, this is difficult when looking at realistic systems, such as polycrystalline materials. Grain boundaries (GBs) are challenging to model due to the sheer number of macroscopic and microscopic degrees of freedom required to mathematically describe such interfaces (Bean & McKenna, 2016; Saylor et al., 2004; Saylor et al., 2003). The primary type of GB modelled atomistically, is known as a 'bi-crystal', which contains two grains and a single type of interfacial orientation relationship between those grains (Bean et al., 2017; Prakash et al., 2016). However, in real materials, millions of grains could have a similar number of orientational relationships. Designing and developing new materials using computational methods alone requires accurate representations of the complete grain structure, coupled with accurate methods of atomic interactions.

Recently, methods which enable the construction of the complex grain structure of polycrystalline materials based on Voronoi tessellations (VT) have been developed. The 'NanoSCULPT' method can construct complex polycrystals with an arbitrary number of grains (Prakash et al., 2016; Prakash et al., 2017). Using the VT method presents several different challenges which still need to be overcome; the first challenge is that the Voronoi method of defining grain structures creates grains which have planar interfaces (Jacob Gruber et al., 2017). Secondly the local structure of the grain boundaries or microscopic degrees of freedom can be significantly different to those generated by the Voronoi tessellations, which can change the interface energy and, stability of the grain boundary. New models which have developed new ways to generate GB microstructures have been proposed. Still, they have not yet been linked to molecular dynamics simulation, which enables predictive power, which is the crucial value of this work (Lazar et al., 2011).

In this work, we developed a grain growth algorithm that can be used in conjunction with NanoSCULPT to construct complex grain structures more representative of real polycrystals. We used robust algorithms (Mason et al., 2015; Panzarino & Rupert, 2014) to produce GB structures with curved GBs. We then determine mechanical properties such as these new systems' bulk modulus and excess volume. It is found that there is a lower formation energy and a comparable extra volume and the magnitude of the elastic moduli is larger for systems with curved GBs than those with planar GBs. In addition, we have used a grain tracking algorithm to determine the number of triple junctions adjacent to each grain boundary (Barber et al., 1996). It has been found that there are systematically more triple junctions in the planar grain boundary networks constructed using Voronoi tessellations than in those made using our grain growth model. Our ability to detect triple junctions gives both a route to compare against experiments and a structural characterisation of the differences between the two types of structures. In addition, anomalous growth of an unexpected close-packed hexagonal (cph) phase occurs in the VT systems, further demonstrating the non-physicality of these systems. Another key value for this work in the context of other research in this direction is that we have developed an easy-to-use way for other researchers to use our tool to construct their systems of grains.

2. Methods

2.1. General approach

In this work, two different methods were employed to construct complex networks of grains. The first method is known as Voronoi tessellation (VT). VT works by generating a 3D network of grains based on an initial number of seed points. Individual grains are constructed as regions of space assigned to the closest seed point. The location of the seed points determines the distribution of grain sizes, and their number is equal to the total number of grains within the structure. GB networks constructed using VT possess GBs which have planar grain boundaries. There is considerable variance associated with the resulting systems, and many other unphysical features, such as quadruple junctions, are sometimes generated. Initial grain centres are caused by a uniform random distribution of points within a predefined volume, from which a Voronoi tessellation is generated using 'Qhull'

(MacPherson & Srolovitz, 2007). This tessellation is then used as input for 'nanoSCULPT', which fills the individual grain volumes with atoms with a selected crystal structure and density. The orientation of the crystal lattice within the grain volumes concerning the cardinal axes is random. GB networks constructed using VT are very unlikely to be representative of real materials.

The second method, called grain growth (GG), uses a code which was developed to optimise an initial vertex map based on macroscopic models of grain boundaries (Mason et al., 2015). This GG method ensures that the microstructure evolution follows the MacPherson–Srolovitz (M-S) relation (Cheng et al., 2009). The M-S relation ensures that the grain boundary growth dynamics is thermodynamic and a solution to the Adam-Gibbs equation. Like the VT method, the GG method also outputs a vertex map of the grain boundaries, which is used as input for 'nanoSCULPT' and populated with atoms. In both cases, the same number of grains and average grain sizes have been used to ensure that results can be directly compared.

Note that the lattice constants used for the copper systems presented here were pre-optimised on perfect cells to minimise contraction or expansion following structure creation. Atoms which were too close to another were deleted, with the proximity threshold determined by the atomic radii of the pair of atoms. Three-dimensionally periodic boundary conditions have been used for all simulations throughout the paper.

Schematics of polycrystals constructed using the VT and GG methods are shown in Figs. 1a and 1b. While it is difficult to observe by significant eye curvature when comparing the planar to curved systems, this can be observed through the detection of triple junctions, which is explained in more detail later (see Figs. 3d and 3c).

2.2. Interatomic interactions

To describe interatomic interactions for cubic-close packed (ccp) copper, embedded atom method (EAM) potentials have been used for all systems investigated in this work. The EAMs offer a balance between physical accuracy and computational feasibility. Due to its expense, DFT cannot currently be used for systems sizes greater than ≈ 50,000 electrons or access timescales that are sufficiently long (≈ 1 ns) to model large polycrystalline materials. EAM potentials give an accurate description of bulk, surface and reproduction of experimental properties (Cheng & Ma, 2011; Mendelev et al., 2009; Mendelev et al., 2007). Extensive research has been undertaken using a range of interatomic potentials which have been developed for nanocrystalline materials (Jacob Gruber et al., 2017; Gruber et al., 2017). This study uses the parameterisation of

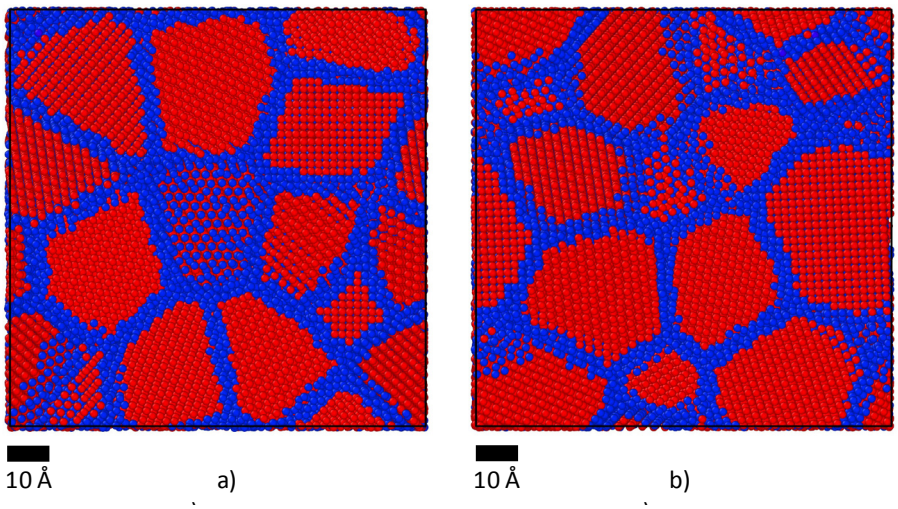

Figure 1. Schematics of different types of grain boundary models which can be constructed. **a)** A model system of planar grain boundaries constructed using Voronoi tessellation and nanoSCULPT. **b)** A model system of curved grain boundaries constructed using grain growth and nanoSCULPT.

Phase	Cohesive Energy (eV/atom)	Volume (A^3)	Theory
cph	-3.15	14.56	DFT
bcc	-3.43	12.05	DFT
ccp	-3.38	12.18	DFT
cph	-3.20	13.44	Sheng-Potential
bcc	-3.51	11.73	Sheng-Potential
ccp	-3.54	11.64	Sheng-Potential
cph	-2.83	12.77	Mendelev-Potential
bcc	-3.24	12.13	Mendelev-Potential
ccp	-3.28	12.05	Mendelev-Potential
ccp	-3.52 (Kambe, 1955)	11.81 (Pearson, 2013)	Experiment

Table 1. Calculated cohesive energies and volume of copper phases using density functional theory, Sheng's interatomic potential and Mendelev's interatomic potential at 0 K.

Howard Sheng for the binary copper-zirconium alloy, which has been broadly applied giving good results including for polycrystalline materials which is the focus of this work (Kambe, 1955; Zhao et al., 2018).

In this work, we have compared different choices of interatomic potentials against DFT to give good accuracy. We find that the Sheng interatomic potential produces results which are in good agreement with DFT and experimental results (see Table 1).

2.3. Optimisation

After the initial construction of GB geometry, there will be atoms in unfavourable energetic positions, even if overlapping atoms are deleted. The effect of these atom overlaps will be residual stresses within the structure, which could result in net contraction or expansion to minimise total pressure within the system. The molecular dynamics code LAMMPS (Plimpton, 1995) was used to optimise the geometry of the systems, achieved through adjusting both the atomic positions and cell vectors to minimise forces, energies and pressures. Optimisation is required to calculate elastic and plastic properties, which cannot be done reliably if the system is not at an energy minimum. We use the conjugate gradient method for the minimisation to a threshold precision of 1×10^{-8} eV/Å in forces and 1×10^{-8} eV in energies, with a maximum of 100,000 iterations and 1,000,000 computations. The minimisation cell symmetry is fixed as isotropic and was limited to a volume change of 0.001 $Å^3$ per iteration, which is small enough to find close minima and ensure that the cell transformation did not significantly affect the structure during relaxation.

2.4. Elastic properties

There are two types of mechanical properties which can be calculated or measured in materials: elastic properties and plastic properties. The elastic properties describe the reversible mechanical behaviour at minor strains, while the plastic properties characterise the effect of more enormous irreversible strains. In simulations, calculations of elastic properties are vastly more accurate than plastic properties since the former can be calculated in the infinite timescale limit. All elastic properties can be encapsulated in an object known as the elasticity tensor (C_{ij}). The elasticity tensor describes how the material responds to different stresses or strains and can be calculated by taking the gradient of the total energy concerning strains in different directions,

$$C_{ij} = \frac{d^2 E_{ij}}{d\epsilon_i d\epsilon_j} \quad (1)$$

where $\varepsilon_{i,j\ is}$ small strains applied in different directions. 6 possible strains are giving a 36-element tensor, but due to symmetry, there are only 21 independent elements. The number of separate elements of the tensor further reduce when dealing with highly isotropic and homogeneous materials. The elasticity tensor can

be calculated using LAMMPS by imposing small strains on an input cell in different directions.

2.5. Stress/strain curves

After computing the elasticity tensor, it is also possible to compute 'stress/strain' curves for tension and compression. Stress/strain curves show the relationship between the mechanical properties in both the elastic and plastic regimes. As is the case in most MD simulations, due to the speed at which these tests are conducted, the strain rate is significantly higher than in the experiment, so the stress before the materials start to yield is also considerably higher than in experiment. The strain which triggers the breaking condition is protracted since the rate of diffusion and reconstruction of the atomic bonding is comparable to the strain rate. In this work, we have undertaken additional mechanical calculations on the supercells constructed. These simulations were performed again using LAMMPS, where the strain on the supercell was gradually increased at each value of the strain, and the result stress in each direction was then measured. A prediction of the Young's modulus is also made from the gradient of the linear regime of the stress/strain curve. The strain rate in all simulations is set at 1×10^{8} %/s with a maximum strain of 0.3. The Nose-Hoover thermostat and Rahman barostat were used throughout.

2.6. Grain boundary energy and excess volume

In the case of bi-crystal GBs the energy of each GB normalised per unit area can be easily obtained. The same is not true here as we are constructing polycrystalline models with many grain boundaries. To determine the total stability for each polycrystalline system, we use a modified definition of the formation energy, given as,

$$\gamma = \frac{E_{tot} - NE_{coh}}{N}, \tag{2}$$

where E_{tot} is the optimised total energy of the supercell, N is the number of atoms in the supercell, and E_{coh} is the bulk cohesive energy. The formation energy, in this case, is normalised against the total number of atoms in the system, allowing for comparison between planar and curved systems with different volumes and numbers of atoms.

Similarly to the GB energy, the excess volume cannot easily be calculated for individual grains in the system and thus is calculated by taking the difference in total volume and the volume of the perfect ccp Cu lattice, defined as,

$$\delta V = \frac{V_{tot} - N\Omega_{bulk}}{N} \tag{3}$$

where V_{tot} is the volume of the supercell and Ω_{bulk} is the volume per atom in the bulk crystal.

2.7. Triple junction identification

It is straightforward to determine the atoms associated with grain boundaries using common neighbour analysis (CNA) techniques. Still, it is complicated to determine those which are triple junctions (i.e., the intersection of three grains) (Xu & Li, 2010). The number of triple junctions in the polycrystalline models can be used as a metric of similarity to real polycrystalline materials, as this can be experimentally measured using techniques such as Mössbauer spectroscopy. In this work, we have implemented a method originally proposed by (Xu & Li, 2010) which is also known as the 'outward layering method', which indexes all the grains as a function of distance from a grain centre, and concentric layers are then drawn relative to the grain centres. The following conditions are imposed to determine whether an atom is near a triple junction:

- If the grain index (GI) of an atom and its neighbours are the same, then it is an atom located inside that grain (called a 'atom')
- If an atom and its neighbours have two different GIs, it is a grain boundary atom.
- If an atom and its neighbours have three different GIs, it is a grain boundary triple junction atom.
- If an atom and its neighbours have four or more different GIs, then it is a vertex atom.

A MATLAB script initially developed by (Panzarino & Rupert, 2014) was adapted to perform calculations in this work. The script inputs the atomic coordinates of the system in question, along with the common neighbour analysis result and the centrosymmetric parameter

(Kelchner et al., 1998). The script then returns a number between 0 and 7, characterising how 'triple-junction-like' an atom is. In this work, we consider atomic environments which are triple-junction-like to be greater than or equal to 6.

3. Results

The previously described methods create GB networks of planar and curved GBs of average grain size between 1.9nm and 3nm, with each grain filled with single-phase ccp Cu. The total number of grains in each system was initialised at 50 to allow for a like-for-like comparison between planar and curved GB systems for each system size. The average grain size is estimated from the system's total volume and the number of grains in the system. For each system, the elastic, tensile, energetic, and volumetric properties are calculated, as well as the number of triple junctions.

The results of the elastic property calculations are shown in Table 2. The bulk modulus is approximately constant with increasing grain size within a variation of ±10% for both the planar, and curved systems. For the shear modulus, there is a marked increase with increasing grain size for both planar and curved systems. The growth in the shear modulus may be related to the decreasing fraction of GB area as the grain size increases, but the number of grains is held constant. A reduced GB area would mean less GB sliding, a crucial resistance mechanism against shear. This increase in the shear modulus with grain size may be a novel relationship, which could be important for designing new materials. For Poisson's ratio, there is a slight reduction with grain size. Interestingly, the trends associated with the elastic properties are repeated for the planar and curved grain boundaries with only small differences between absolute values. This suggests that the elastic properties are not significantly affected by the nature and type of grain boundaries within these kinds of systems.

Some randomisation is associated with the construction of the GB networks. To minimise this, a total of 5 different systems for both planar and curved GBs were additionally constructed for the 2.71 nm average grain size, to show the statistical significance of the results found, the average and standard deviation are shown for the elastic properties of this system in Table 3. On average, the curved systems possess a larger bulk modulus by approximately 2 standard deviations, consistent with the results upon increasing the grain size (Table 2). For the shear modulus, the curved GBs is more excellent by over 3 standard deviations, which is also consistent with the results found for increasing grain size. At the same time, the results are not exactly as those which appear in Table 1, it shows a statistically significant difference between planar and curved systems, with curved systems being far more robust in terms of shear and bulk moduli.

While static properties of materials can be easily and accurately calculated using atomistic simulations involving small strains at infinitesimal timescales, plastic properties are more difficult due to the long timescales associated with deformation processes compared to structural relaxation. To complement the elastic results, plastic 'tensile' simulations were performed on the systems of planar and curved GB structures to understand the high-strain deformation behaviour and associated stresses. Results of these simulations, for example, methods are shown in Fig. 2.

Average grain size (nm)	No. grains	GB type	Poisson's ratio	Bulk modulus (GPa)	Shear modulus (GPa)
2.98	50	planar	0.377	126.08	33.74
2.98	50	curved	0.376	134.20	36.42
2.71	50	planar	0.388	126.47	30.68
2.71	50	curved	0.380	131.52	34.39
2.44	50	planar	0.391	135.40	31.78
2.44	50	curved	0.400	150.01	32.39
2.17	50	planar	0.402	134.47	28.05
2.17	50	curved	0.401	132.77	28.11
1.90	50	planar	0.429	128.80	19.14
1.90	50	curved	0.418	137.92	23.87

Table 2. Elastic properties for different system sizes of planar and curved grain boundary systems.

Average grain size (nm)	GB type	Poisson's ratio	Bulk modulus (GPa)	Shear modulus (GPa)
2.71	Planar	0.380±0.003	128.54±0.84	33.50±1.14
2.71	Curved	0.371±0.002	130.12±0.73	36.83±0.58

Table 3. Elastic properties for planar and curved grain boundary systems.

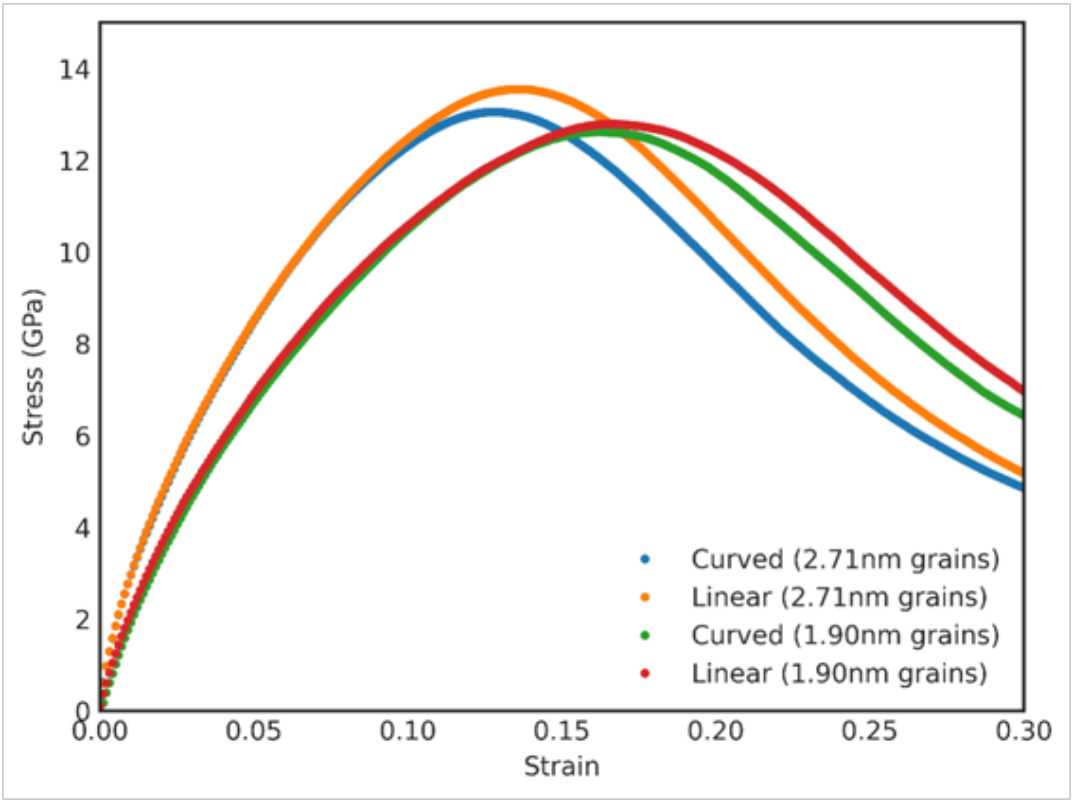

Figure 2. Stress/strain curves for 'tensile' tests performed on nanocrystalline models with different grain boundaries.

When comparing the difference between the planar and curved grains systems, the planar grains surprisingly result in higher yield stress. This is surprising since the modulus is lower. This result could be because the planar system contains more dislocations, effectively work-hardening the system.

The phenomena exhibited by changing the system size seem to agree with the conventional Hall-Petch equation (Hall, 1951), where a decrease in grain size results in strengthening rather than weakening. As with most MD simulations of yielding, there is no well-defined breaking condition because the timescale of atomic motion is comparable to the strain rate. If very long timescale tension simulations were performed, then the atomic relaxation would be fast relative to the deformation rate such as. The system would yield a different strain. This is further compounded due to the pressure dependence of elastic properties. In all cases, there is a non-zero value of stress at zero strain due to the imperfect minimisation of the initial structures.

The GB energies and excess volumes for the 2.71 nm average grain size system are shown in Table 4. For this system, the curved GBs have smaller formation energy but similar excess volume when compared to the planar GBs. The smaller formation energies indicate that the curved GB models are more energetically stable. The fact that the extra volumes associated with the two different types of materials are comparable

Average grain size (nm)	GB type	Formation energy (eV)	Excess volume (Å^3)
2.71	Planar	0.431±0.017	0.087±0.004
2.71	Curved	0.397±0.014	0.086±0.010

Table 4. Excess volumes and total grain boundary energies of planar and curved grain boundary systems.

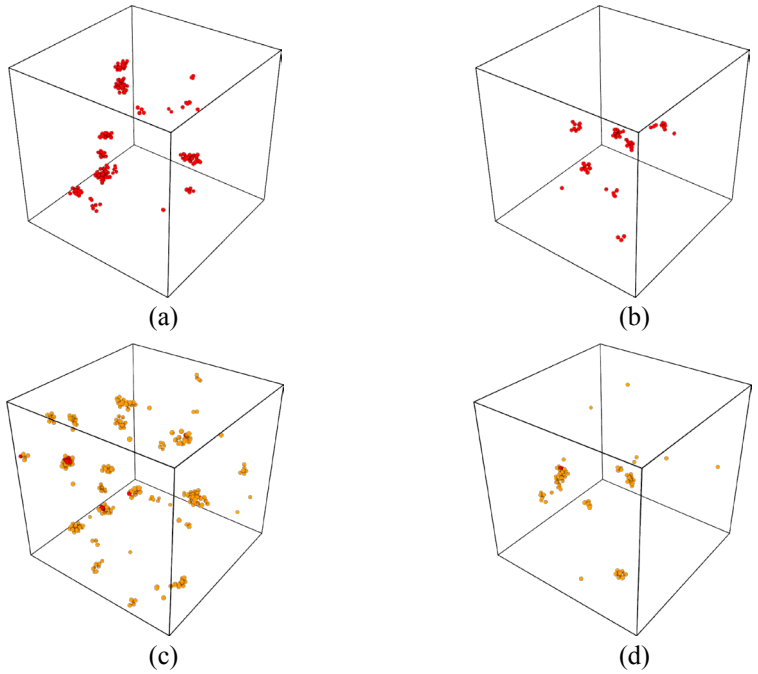

Figure 3. Highlighted triple junctions within grain boundary models. **a)** Grain boundary triple junctions for a system created using the Voronoi tessellation method with planar grain boundaries before relaxation. **b)** Grain boundary triple junctions for a system created using our new grain growth method with curved grain boundaries before relaxation. **c)** Grain boundary triple junctions for a system created using the Voronoi tessellation method with planar grain boundaries after relaxation. **d)** Grain boundary triple junctions for a system created using our new grain growth method with curved grain boundaries after relaxation.

is interesting since there is a linear correlation between energy and volume in a perfect system using a harmonic potential. This departure from that relation shows the significance of anisotropy associated with different GB networks.

The grain tracking algorithm was applied to the 10 planar and curved GB systems of 2.71 nm average grain size to determine whether the nature of triple junctions was different. The number of triple junctions was compared before and after optimisation to understand how geometry minimisation affects the structure. In the case of the planar GB system, the number of triple junctions increases during the optimisation process, while in the curved system, it decreases (see Figs. 3c and 3d). This suggests that the initial geometry specified by VT is further away from equilibrium and, thus, less experimentally relevant.

When comparing planar to curved systems, it was found that there are more triple junctions in the systems constructed using Voronoi tessellation than grain growth (see Table 5). Triple junctions generally are more thermodynamically unstable than atoms at the grain boundaries or within grains and are likely to be annealed out during the grain growth process. A system with more triple junctions is likely to be more nonphysical than another system with fewer junctions.

In addition to determining the mechanical properties of the polycrystalline materials, long-timescale simulations were performed to understand their grain growth behaviour.

Average grain size (nm)	GB type	Triple junctions (theoretical)	Triple junctions (model)
2.71	Planar	5%	2.22±0.08 %
2.71	curved	5%	1.09±0.25 %

Table 5. The percentage of atoms in triple junction positions is compared with theoretical and the model system.

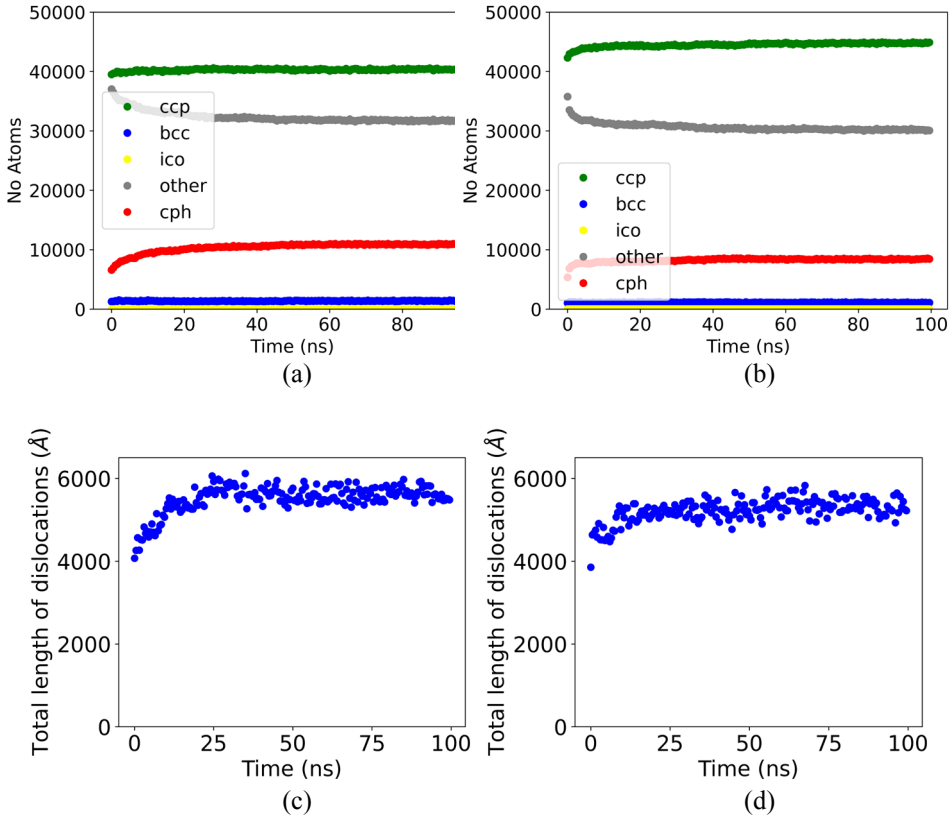

Figure 4. Variation of dislocations and crystal structure of planar and curved grain boundary models over time. Both models were annealed for 100 ns at 300 K in the NPT ensemble. **a)** atomic environment variation of the nanocrystalline grain growth model. **b)** Atomic environment variation of nanocrystalline Voronoi tessellation model. **c)** Total length of dislocations within the nanocrystalline model constructed using our new grain growth method. **d)** Total length of dislocations within the nanocrystalline model constructed using Voronoi tessellation.

Structures of the VT and GG models were annealed for 100 ns at 300 K and 0 GPa using the NPT ensemble, with a total of 200 structural snapshots taken over the trajectory. Two analyses were performed using OVITO (Stukowski, 2010): dislocation analysis, where the types and total lengths of dislocations present in the structure were determined using the DXA method, and joint neighbour analysis (CNA) to identify crystal structures. The results of these analyses are shown in Fig. 4. It is observed that the systems constructed using the Voronoi tessellation exhibit a larger rate of change of both total lengths of dislocations and atomic environments, the cph crystal structure.

The increased number of dislocations and rate of change of structure indicates that the initial structure is fundamentally more unstable in the Voronoi tessellation model. Interestingly, the two structures start with a similar number of ccp and other coordinated atoms. Still, as time progresses, there is a strong growth in ccp atoms in the grain growth model, with the Voronoi tessellation model

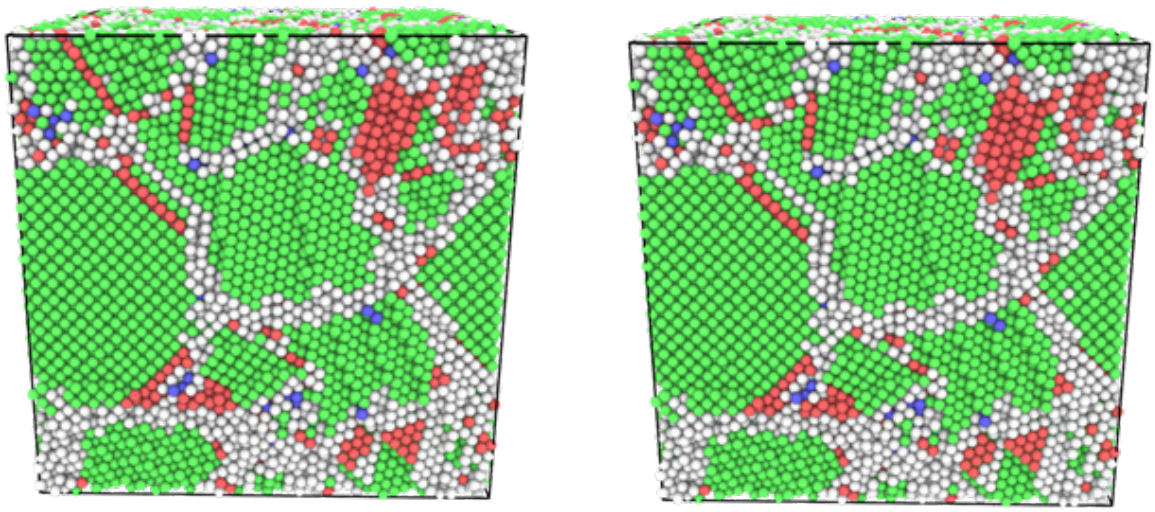

(a) (b)

Figure 5. Schematics of the different grain boundary models after 100 ns of annealing at 300 K (green: ccp, red: cph, blue: bcc, and white: unknown). **a)** Structure of a system constructed using the grain growth model after annealing. **b)** Structure of a system constructed using Voronoi tessellation after annealing.

exhibiting stronger growth in the number of cph-like atoms. Interestingly, in the case of the model constructed using Voronoi tessellation, abnormal growth of the cph phase during the annealing process, which is not present in the grain growth model. There is a non-negligible formation of the cph phase using the grain growth model, which is primarily manifested as stacking faults (see Fig. 5).

4. Discussion

One of the significant challenges when constructing GB networks is that the formation of grains from vertices can yield GBs which are extremely energetically unstable. To overcome this issue, we first deleted atoms that were too close to their neighbours, then minimise the geometry. The optimisation process could slightly destroy the crystal order created in the first instance. This could be a significant effect, but the agreement between results of different sizes of the excess volume difference suggests that much of the underlying geometry remains after the optimisation process. As the relaxation proceeds, the boundaries in the VT GB network become slightly curved, but since the curved grain boundaries are in a lower initial minimum than the planar GBs they are more likely to find a lower minimum after relaxation (see Table 4). The performance of interatomic potentials is significant for the accurate prediction of properties of atomic systems. Still, in this work, as we are comparing the performance of two different structural models with the same potential, the shortcomings of the potential are unlikely to impact the comparison. When the number of triple junctions was measured before and after relaxation, only a small difference was detected, giving further confidence in the results.

The grain size for the model systems in this study range from 1.5-3 nm. The small grain size increases the fraction of atoms in the vicinity of the grain boundaries, which could amplify the effects associated with the difference between planar and curved grain boundaries. Since we determine that the fraction of atoms at triple junctions is significantly different between the two types of systems, we have further confidence in the method's reliability. The common neighbour analysis further reveals the systematic differences between the two kinds of GB.

The interatomic potential we have used throughout this paper has been used extensively throughout the academic literature, including for simulations involving grain boundaries.

The Hall-Petch effect asserts that there will be 'grain boundary hardening', where decreasing the grain size makes the material stronger. For grain sizes below 10 nm an 'inverse Hall-

Petch' relationship has been detected (Carlton & Ferreira, 2007). However, in this work, we find at grain sizes of 3 nm and less that, there is no inverse Hall-Petch relationship, and only the standard form exists. This is interesting because experimentally, it is difficult to create samples with a very small grain size, and imaging the samples or verifying this would be a further challenge. The results in this work may suggest another regime of Hall-Petch, where the effect seems to revert after the inversion as the interplay of defects changes. Additional work investigating how temperature affects the mechanical properties of these systems may shed further light on the Hall-Petch effect and its origins.

In this work, we have used the conventional method of Voronoi tessellation to construct GB networks. It may be possible to improve the VT method by using 'Poisson-disk sampling' (Tschopp & McDowell, 2007) rather than a uniform random distribution to generate initial grain centres, however, this will not avoid the problem of creating planar grain boundaries and thus a large number of triple junctions and higher numbers of vertices than would be experimentally detected.

Another key area to improve the results in this work is to understand further the impact of the orientations of the crystal structures inserted into the grains. In both VT and GG constructions, random rotations were used, and it is quite likely that there are more favourable and physically motivated distributions of rotations between the grains, which may increase the realism of the constructed systems and allow the discovery of deeper minima upon relaxation.

While the GG method is powerful, it assumes that the grain boundary energies associated with every orientation are constant, which for certain high-symmetry grain boundaries will be incorrect (Zhao et al., 2010). On average, the GG method will give more realistic results when compared to VT, particularly about the distribution of total length of dislocations, a possible source for the differences between the mechanical properties found in the structures generated by each method.

This work has some ambiguity associated with the recognition of triple junctions against vertices. Due to the nanocrystalline nature of the systems constructed, the length of the triple lines is small, and thus they can easily be misinterpreted as vertices. Fundamentally this does not change any of the conclusions in this work, but comparing against experiments for such small systems, comparisons against vertices should be performed rather than triple junctions.

5. Conclusion

In this work, we have developed a new method to construct polycrystalline materials based on a realistic representation of a grain boundary network. We have used this new method to investigate the difference between polycrystals constructed using the planar grain boundaries concept, and those with curved grain boundaries. One surprising result revealed by the analysis is the differences associated with the number of GB triple junctions identified between planar and curved systems, the latter containing fewer. Experimental verification may be possible for several results, such as the relationship between triple junctions and shear modulus. For other results, such as the relationship between mechanical properties and different grain sizes and a number of grains, experimental investigations may be more difficult due to the challenge of creating samples containing specific grain sizes. However, the nature of curved grain boundaries has been observed in transmission electron microscopy, which gives us confidence in our method.

A linear correlation was observed between the shear modulus and grain size ($\mu \propto d$), which could be a significant result in designing nanocrystalline materials with specific properties. Furthermore, it has been found that there is no inversion of the Hall-Petch relationship at grain sizes investigated in this work (less than 3 nm), however, further investigation is required to determine if this is a new regime or evidence against the existence of an 'inverse-Hall-Petch' relationship.

In addition, it has been found that the grain growth behaviour is significantly different between the two models, with the traditional VT model exhibiting more growth of cph structures compared to the GG model, which grows more ccp environments. This result may be coupled to the different total length of dislocations, which is longer within structures created via the VT model

suggesting a source for the diminished mechanical properties.

Acknowledgements

We want to acknowledge financial support from the ERC (RG/80944). Thanks to A.L. Greer for the helpful discussions.

SG acknowledges the financial support provided by the UKRI via Grants No. EP/S036180/1, EP/T001100/1 and EP/T024607/1, feasibility study awards to LSBU from the UKRI National Interdisciplinary Circular Economy Hub (EP/V029746/1) and Transforming the Foundation Industries: a Network+ (EP/V026402/1), the Hubert Curien Partnership award 2022 from the British Council, Transforming the Partnership award from the Royal Academy of Engineering (TSP1332) and the Newton Fellowship award from the Royal Society (NIF\R1\191571). This work also accessed the Isambard Bristol, UK supercomputing service via Resource Allocation Panel (RAP) and ARCHER2 resources (Project e648).

We also acknowledge facilities support provided by the Cambridge Service for Data Driven Discovery (CSD3) operated by the University of Cambridge Research Computing Service (http://www.csd3.cam.ac.uk/), provided by Dell EMC and Intel using Tier-2 funding from the EPSRC (capital grant EP/P020259/1), and DiRAC funding from the STFC (www.dirac.ac.uk). Please contact the authors to obtain the software to generate further polycrystalline systems.

References

Ashby, M. F., & Jones, D. R. (2011). *Engineering materials 1: an introduction to properties, applications and design* (Vol. 1): Elsevier.

Ashby, M. F. J. M. I. (1994). Materials selection in mechanical design. *86*, 475-475.

Barber, C. B., Dobkin, D. P., & Huhdanpaa, H. J. A. T. o. M. S. (1996). The quickhull algorithm for convex hulls. *22*(4), 469-483.

Bean, J. J., & McKenna, K. P. J. A. M. (2016). Origin of differences in the excess volume of copper and nickel grain boundaries. *110*, 246-257.

Bean, J. J., Saito, M., Fukami, S., Sato, H., Ikeda, S., Ohno, H., . . . McKenna, K. P. J. S. r. (2017). Atomic structure and electronic properties of MgO grain boundaries in tunnelling magnetoresistive devices. *7*(1), 1-9.

Carlton, C., & Ferreira, P. J. A. M. (2007). What is behind the inverse Hall–Petch effect in nanocrystalline materials?, *55*(11), 3749-3756.

Cheng, Y., Ma, E., & Sheng, H. J. P. r. l. (2009). Atomic level structure in multicomponent bulk metallic glass. *102*(24), 245501.

Cheng, Y., & Ma, E. J. P. i. m. s. (2011). Atomic-level structure and structure–property relationship in metallic glasses. *56*(4), 379-473.

Gruber, J., Lim, H., Abdeljawad, F., Foiles, S., & Tucker, G. J. J. C. M. S. (2017). Development of physically based atomistic microstructures: the effect on the mechanical response of polycrystals. *128*, 29-36.

Gruber, J., Zhou, X., Jones, R., Lee, S., & Tucker, G. (2017). Molecular dynamics studies of defect formation during heteroepitaxial growth of InGaN alloys on (0001) GaN surfaces. *Journal of Applied Physics, 121*(19), 195301.

Hall, E. J. P. o. t. P. S. S. B. (1951). The deformation and ageing of mild steel: III discussion of results. *64*(9), 747.

Hirth, J. J. M. T. A. (1985). A brief history of dislocation theory. *16*(12), 2085-2090.

Jones, D. R., & Ashby, M. F. (2012). *Engineering materials 2: an introduction to microstructures and processing*: Butterworth-Heinemann.

Kambe, K. J. P. R. (1955). Cohesive energy of noble metals. *99*(2), 419.

Kelchner, C. L., Plimpton, S., & Hamilton, J. (1998). Dislocation nucleation and defect structure during surface indentation. *Physical Review B, 58*(17), 11085.

Lazar, E. A., Mason, J. K., MacPherson, R. D., & Srolovitz, D. J. J. A. M. (2011). A more accurate three-dimensional grain growth algorithm. *59*(17), 6837-6847.

MacPherson, R. D., & Srolovitz, D. J. J. N. (2007). The von Neumann relation generalized to coarsening of three-dimensional microstructures. *446*(7139), 1053-1055.

Mason, J. K., Lazar, E. A., MacPherson, R. D., & Srolovitz, D. J. J. P. R. E. (2015). Geometric and topological properties of the canonical grain-growth microstructure. *92*(6), 063308.

Mendelev, M., Kramer, M., Ott, R., Sordelet, D., Yagodin, D., & Popel, P. J. P. M. (2009). Development of suitable interatomic potentials for simulation of liquid and amorphous Cu–Zr alloys. *89*(11), 967-987.

Mendelev, M., Sordelet, D., & Kramer, M. J. J. o. A. P. (2007). Using atomistic computer simulations to analyze x-ray diffraction data from metallic glasses. *102*(4), 043501.

Orowan, E. J. Z. P. (1934). The crystal plasticity. III: about the mechanism of the sliding. *89*, 634-659.

Panzarino, J. F., & Rupert, T. J. J. J. (2014). Tracking microstructure of crystalline materials: a post-processing algorithm for atomistic simulations. *66*(3), 417-428.

Pearson, W. B. (2013). *A handbook of lattice spacings and structures of metals and alloys: International series of monographs on metal physics and physical metallurgy, Vol. 4* (Vol. 4): Elsevier.

Plimpton, S. (1995). Fast Parallel Algorithms for Short-Range Molecular Dynamics. *Journal of Computational Physics, 117*, 1-19.

Prakash, A., Hummel, M., Schmauder, S., & Bitzek, E. J. M. (2016). Nanosculpt: A methodology for generating complex realistic configurations for atomistic simulations. *3*, 219-230.

Prakash, A., Weygand, D., & Bitzek, E. J. I. J. o. P. (2017). Influence of grain boundary structure and topology on the plastic deformation of nanocrystalline aluminum as studied by atomistic simulations. *97*, 107-125.

Saylor, D. M., El Dasher, B. S., Rollett, A. D., & Rohrer, G. S. J. A. M. (2004). Distribution of grain boundaries in aluminum as a function of five macroscopic parameters. *52*(12), 3649-3655.

Saylor, D. M., Morawiec, A., & Rohrer, G. S. J. A. m. (2003). The relative free energies of grain boundaries in magnesia as a function of five macroscopic parameters. *51*(13), 3675-3686.

Stukowski, A. (2010). Visualization and analysis of atomistic simulation data with OVITO–the Open Visualization Tool. *Modelling and Simulation in Materials Science and Engineering, 18*(1).

Sutton, A. P. J. M. o. t. P., & Materials, C. o. (1995). Interfaces in crystalline materials. 414-423.

Tschopp, M., & McDowell, D. J. P. M. (2007). Structures and energies of Σ 3 asymmetric tilt grain boundaries in copper and aluminium. *87*(22), 3147-3173.

Xu, T., & Li, M. J. P. M. (2010). Geometric methods for microstructure rendition and atomic characterization of poly-and nano-crystalline materials. *90*(16), 2191-2222.

Zhao, B., Verhasselt, J. C., Shvindlerman, L., & Gottstein, G. J. A. m. (2010). Measurement of grain boundary triple line energy in copper. *58*(17), 5646-5653.

Zhao, L., Chan, K. C., & Chen, S. J. I. (2018). Atomistic deformation mechanisms of amorphous/polycrystalline metallic nanolaminates. *95*, 102-109.